



Parametric Decay Instability and Dissipation of Low-frequency Alfvén Waves in Low-beta Turbulent Plasmas

Xiangrong Fu¹ , Hui Li², Fan Guo² , Xiaocan Li² , and Vadim Roytershteyn³

¹New Mexico Consortium, Los Alamos, NM 87544, USA; sfu@newmexicoconsortium.org

²Los Alamos National Laboratory, Los Alamos, NM 87545, USA

³Space Science Institute, Boulder, CO 80301, USA

Received 2017 November 9; revised 2018 January 30; accepted 2018 January 31; published 2018 March 16

Abstract

Evolution of the parametric decay instability (PDI) of a circularly polarized Alfvén wave in a turbulent low-beta plasma background is investigated using 3D hybrid simulations. It is shown that the turbulence reduces the growth rate of PDI as compared to the linear theory predictions, but PDI can still exist. Interestingly, the damping rate of the ion acoustic mode (as the product of PDI) is also reduced as compared to the linear Vlasov predictions. Nonetheless, significant heating of ions in the direction parallel to the background magnetic field is observed due to resonant Landau damping of the ion acoustic waves. In low-beta turbulent plasmas, PDI can provide an important channel for energy dissipation of low-frequency Alfvén waves at a scale much larger than the ion kinetic scales, different from the traditional turbulence dissipation models.

Key words: instabilities – solar wind – turbulence – waves

1. Introduction

An Alfvén wave is a fundamental magnetohydrodynamic (MHD) mode that prevails in laboratory, space, and astrophysical plasmas. In solar corona and solar wind, Alfvén waves are ubiquitous as a major carrier of fluctuating magnetic energy. They are often observed to have large amplitudes so that nonlinear wave–wave and wave–particle interactions are expected to be important (Tu & Marsch 1995).

It is rare to observe narrowband Alfvén waves in the solar wind. Instead, measured magnetic fluctuations are mostly turbulent, in the sense that the energy spreads across a wide range of frequency, typically over 3–4 orders of magnitude. This is believed to be a result of nonlinear wave–wave interaction among counter-propagating Alfvén packets (Goldreich & Sridhar 1995), where long-wavelength perturbations are cascading into short-wavelength ones and form a power-law energy spectrum from the injection scale down to ion kinetic scales (ρ_i or d_i) (e.g., Howes 2015).

On the other hand, in compressible plasmas, large amplitude Alfvén waves (and magnetosonic waves) are subject to a parametric decay instability (PDI)—another category of nonlinear wave–wave interactions—where a forward-propagating Alfvén wave (pump wave) decays into a backward-propagating Alfvén wave and a forward-propagating ion acoustic wave or slow wave. (Note that, in the paper, we use the terms “slow mode” and “ion acoustic mode” interchangeably in low-beta plasmas, see Gary (1993) and Verscharen et al. (2017) for relations between these two modes.) PDI provides not only a robust mechanism for generating backward-propagating waves, which are a key ingredient in the turbulence cascading process mentioned above, but also a mechanism to dissipate wave energy into plasma through Landau damping of ion acoustic waves. This dissipation of energy can be efficient because it occurs at a fluid scale (comparable to the wavelength of Alfvén waves, $kd_i \ll 1$), in contrast to dissipation at ion kinetic scales where the energy budget is much smaller.

There have been comprehensive theoretical and simulation studies on parametric decay instabilities of Alfvén waves in

quiescent plasmas in the literature. The PDI of the linearly polarized Alfvén wave in the limit of small pump wave amplitude ($\delta B/B_0$) and low plasma beta (β) was studied by Sagdeev & Galeev (1969), and its growth rate is

$$\frac{\gamma}{\omega_0} \approx \frac{1}{2} \frac{\delta B}{B_0} \frac{1}{\beta^{1/4}}, \quad (1)$$

where ω_0 is the frequency of the pump wave. For a circularly polarized Alfvén (CPA) wave, the dispersion relation in the MHD limit can be obtained for finite $\delta B/B_0$ and β , as given independently by Derby (1978) and Goldstein (1978). The dependence of the pump wave amplitude on plasma beta for various maximum growth rates of PDI $\gamma_{\max}/\omega_0 = 0.01, 0.05, 0.10$ (by solving Equation (17) of Derby 1978) are shown in Figure 1. It is clear that the threshold amplitude of PDI is low in low-beta plasmas, e.g., an Alfvén wave with an amplitude as small as 10^{-2} will be unstable when $\beta < 10^{-2}$.

The nonlinear features of PDI have been investigated by numerical simulations, including MHD and hybrid simulations, for monochromatic (Gao et al. 2013b) and nonmonochromatic Alfvén waves (Malara et al. 2000), at parallel and oblique propagation (Zanna 2001; Matteini et al. 2010), in multiple dimensions (Matteini et al. 2010; Gao et al. 2013a), with multiple ion species (Gao et al. 2013b), and in expanding solar wind (Tenerani & Velli 2013; Del Zanna et al. 2015). These studies focused on PDI in quiescent plasmas. PDI in turbulent plasmas had not been explored until recently. Using 3D MHD simulations, Shi et al. (2017) found that PDI can survive turbulence over a broad range of parameters, only with growth rates reduced by about 50%. But kinetic effects were missing in their study due to the limitation of the MHD model. Can PDI survive in a more realistic turbulent environment? In this study, we address this question using 3D hybrid simulations with full ion kinetics, while still retaining large-scale turbulence in the inertial range. In a turbulent warm plasma, the growth and damping of various plasma waves predicted by the linear Vlasov theory may be altered significantly, challenging the

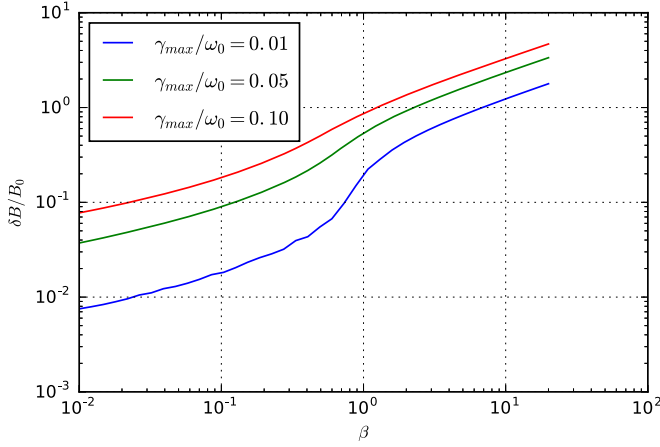


Figure 1. Dependence of the pump wave amplitude on the plasma beta for various maximum growth rates of PDI $\gamma_{\max}/\omega_0 = 0.01, 0.05, 0.10$.

effectiveness of parametric decay on ion heating of ions, which is also addressed in the current paper.

The main evidence of PDI in space plasmas is the presence of slow modes in in situ measurements (Tu & Marsch 1995 and references therein). Spangler et al. (1997) reported a signature in the field and density spectra consistent with the PDI theory in the upstream of the Earth's bow shock. Slow modes have been identified in various analyses of solar wind data (e.g., Kellogg & Horbury 2005; Howes et al. 2012; Yao et al. 2013). Recently, Shi et al. (2015) analyzed data from WIND spacecraft in Solar Cycle 23, and found the existence of slow waves in 3.4% of the selected time period, preferentially in moderate-speed solar wind. However, in general, nonlinear wave-wave interactions are difficult to pin down (Narita & Glassmeier 2007). In laboratory experiments, a parametric instability of a finite ω/Ω_i kinetic Alfvén wave (modulational instability) was recently directly observed for the first time on the Large Plasma Device (Dorfman & Carter 2016); but verification of the classic PDI remains challenging.

2. Simulation Model

We use a hybrid simulation (kinetic ions and mass-less fluid electrons) to study the parametric decay of large amplitude Alfvén waves in low-beta turbulent electron-proton plasmas. The hybrid model is appropriate because we focus on energy dissipation at long wavelength ($k d_i \ll 1$). A 3D hybrid code H3D (Karimabadi et al. 2006; Podesta & Roytershteyn 2017) is used in this study with the following typical parameters: $L_x = L_y = L_z/4 = 120d_i$, $N_x = N_y = N_z = 480$, $\Delta t \Omega_i = 0.025$, $\beta_i = 0.01$. The simulation box is elongated to facilitate the development of anisotropic ($k_\perp \gg k_\parallel$) MHD turbulence (Goldreich & Sridhar 1995). Typically 64 marker particles in each cell are used to represent protons. To ensure that our results are not sensitive to the numerical noise, selected simulations with a higher number of particles per cell (NPPC) are also carried out. The plasma is immersed in a uniform background magnetic field $\mathbf{B}_0 = B_0 \mathbf{z}$. Periodic boundary conditions for fields and particles are applied. Electrons have the same temperature as ions initially, and follow an adiabatic equation of state $T_e/n_e^{\Gamma-1} = \text{const}$, where $\Gamma = 5/3$. A small uniform resistivity $\eta_e = 10^{-8} 4\pi/\omega_{pi}$ is assumed. Total energy is conserved within a few percent in all simulations presented. Key parameters for our 3D hybrid simulations are summarized in Table 1.

Table 1
Key Parameters for 3D Hybrid Simulations

Run	Number of Cells	β_i	a_0	a_1	$t_1 \Omega_i$	NPPC
0	$480 \times 480 \times 480$	0.01	0.0	0.1	0	64
1	$480 \times 480 \times 480$	0.01	0.1	0.1	500	64
2	$480 \times 480 \times 480$	0.01	0.1	0.0	N/A	64
3	$480 \times 480 \times 480$	0.01	0.1	0.1	500	216
4	$120 \times 120 \times 480$	0.01	0.1	0.1	500	64
5	$120 \times 120 \times 480$	0.3	0.3	0.3	500	64
6	$120 \times 120 \times 480$	0.3	0.3	0.0	N/A	64

Note. The domain size is $120 \times 120 \times 480 d_i^3$ for all runs. a_0 is the amplitude of large-scale Alfvén waves producing background turbulence. a_1 is the amplitude of injected Alfvén wave and t_1 is the injection time. NPPC is the number of particles per cell.

At $t = 0$, three pairs of counter-propagating long-wavelength Alfvén waves are loaded throughout the simulation domain so that the fluctuating magnetic and velocity fields are (Makwana et al. 2015)

$$\delta \mathbf{B}/B_0 = \sum_{j,k} a_0 \cos(jk_0 y + kk_0 z + \phi_{j,k}) \hat{\mathbf{x}} + \sum_{l,n} a_0 \cos(lk_0 x + nk_0 z + \phi_{l,n}) \hat{\mathbf{y}} \quad (2)$$

$$\delta \mathbf{v}/v_A = \sum_{j,k} a_0 \text{sgn}(k) \cos(jk_0 y + kk_0 z + \phi_{j,k}) \hat{\mathbf{x}} + \sum_{l,n} a_0 \text{sgn}(n) \cos(lk_0 x + nk_0 z + \phi_{l,n}) \hat{\mathbf{y}}, \quad (3)$$

where $(j, k) = (4, 1); (8, 1); (12, -2)$, $(l, n) = (4, -1); (-8, -1); (-12, 2)$ and $k_0 = 2\pi/L_z = 0.013 d_i^{-1}$. Nonlinear interactions of these waves allow energy cascading to form a power-law turbulent spectrum (Goldreich & Sridhar 1995; Howes 2015). After the turbulence has been established, at $t = t_1$ ($t_1 > \tau_A$, where $\tau_A \equiv L_z/v_A$ is the Alfvén transit time), a CPA wave propagating along the background magnetic field, with $\delta \mathbf{B}/B_0 = a_1 \cos(k_1 z) \hat{\mathbf{x}} + a_1 \sin(k_1 z) \hat{\mathbf{y}}$ and $\delta \mathbf{v}/v_A = -\delta \mathbf{B}/B_0$, is injected (superposed on the existing fields) to excite PDI. For a circularly polarized wave, the magnetic pressure $|\mathbf{B}|^2/8\pi$ is spatially uniform and no ponderomotive force is exerted.

3. Results

An overview of simulation Run 1 is shown in Figure 2(a; solid lines). We start with six Alfvén waves each of which has an amplitude $a_0 = 0.1$. These waves interact with each other causing energy cascade, establishing a background turbulence. Analyses of magnetic field fluctuation (not shown) reveal a power-law spectrum in the direction perpendicular to the background magnetic field with $\delta B^2 \propto k_\perp^{-2}$ extending from $k_\perp d_i = 0.2$ to $k_\perp d_i = 2$ within one Alfvén time ($\tau_A = 480 \Omega_i^{-1}$). The wave power in the parallel direction has a much steeper spectrum, roughly proportional to $k_\parallel^{-2.7}$ in the range $0.04 < k_\parallel d_i < 0.4$, probably due to preferential cascading of MHD turbulence in the perpendicular direction (Goldreich & Sridhar 1995; Howes 2015; Oughton et al. 2015). During the process, the magnetic and electric field energies are decreasing and ions are being heated in both parallel and perpendicular directions, similar to previous MHD and full-PIC simulation results (Makwana et al. 2015, 2016; Zhdankin et al. 2017). The

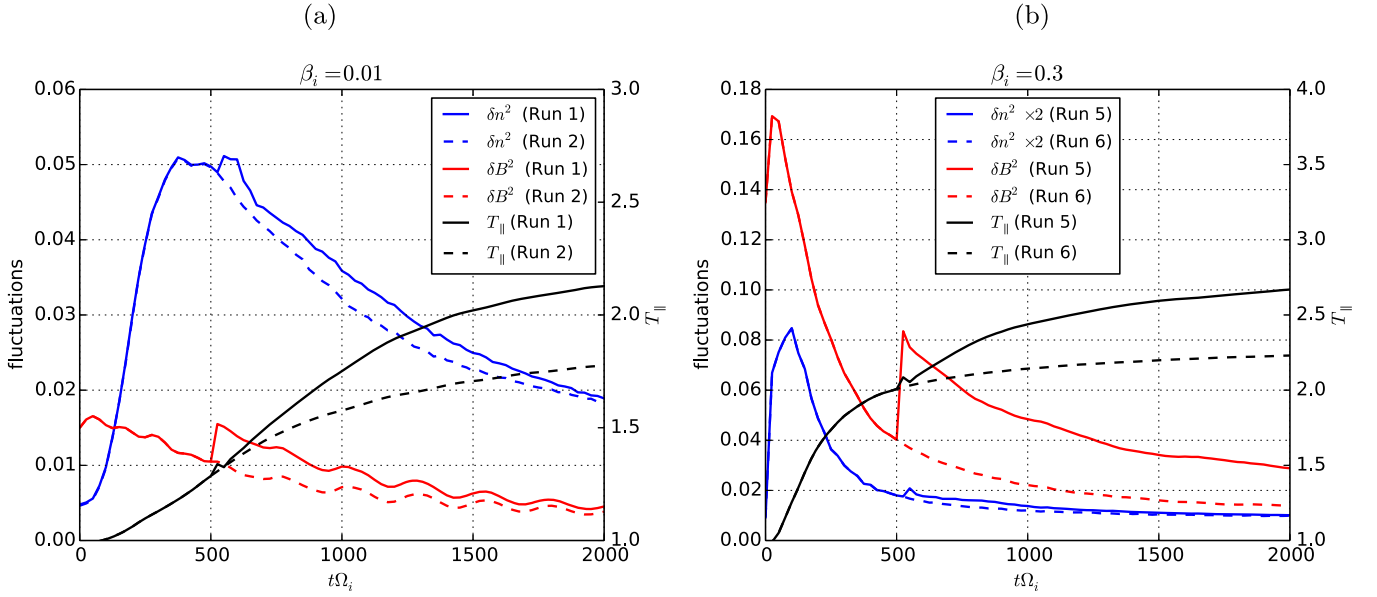


Figure 2. Time evolution of magnetic field fluctuation $(\delta B/B_0)^2$, plasma density fluctuation $(\delta n/n_0)^2$, and parallel ion temperature $T_{\parallel}/T_{\parallel 0}$ in (a) Run 1 and Run 2 with $\beta_i = 0.01$ and (b) Run 5 and Run 6 with $\beta_i = 0.3$. In Run 1 and Run 5, a circularly polarized Alfvén wave is injected at $t\Omega_i = 500$, and no wave is injected in Run 2 or Run 6 after the simulation starts.

density fluctuation also grows and it saturates at $t\Omega_i \approx 400$. At $t = 500\Omega_i^{-1}$, we inject a CPA wave with an amplitude $a_1 = 0.1$ and wavelength $k_1 d_i = 0.13$ into the system. The injection causes an abrupt increase of field energies around $t\Omega_i = 500$. According to the theory of PDI, a slow mode with density perturbation will be excited and the presence of such a mode is evident as the jump in density fluctuation around $t\Omega_i = 500$. For comparison, results of Run 2, which is identical to Run 1, except that no wave is injected after the simulation starts, are shown in dashed curves in Figure 2(a). Although the final turbulence level is close to that of Run 1, parallel ion temperature at the end of Run 2 is significantly smaller than that of Run 1.

In 3D simulations, PDI is free to develop in parallel and oblique directions, as shown in the previous study (Shi et al. 2017). Here we focus on three modes of special interest in Run 1, i.e., modes with $(k_x, k_y, k_z)/k_0 = (0, 0, 10)$, $(0, 0, 7)$, and $(0, 0, 17)$ based on the linear theory of parallel PDI (Derby 1978; Goldstein 1978). Mode $(0, 0, 10)$ is the forward-propagating Alfvén wave (hereafter named Mode 1) injected after the establishment of background turbulence; mode $(0, 0, 7)$ and $(0, 0, 17)$ are the backward-propagating Alfvén wave (Mode 2) and the forward-propagating slow mode (Mode 3) predicted by the linear theory, respectively. Their wave frequencies and wave numbers satisfy the three wave resonance conditions:

$$\omega_1 = \omega_2 + \omega_3, \quad (4)$$

$$\mathbf{k}_1 = \mathbf{k}_2 + \mathbf{k}_3, \quad (5)$$

which are analogous to energy and momentum conservations in quantum mechanics (if multiplied by \hbar). Figures 3(a) and (b) show the evolution of the wave power of perpendicular magnetic field component B_x and density fluctuation δn of these modes. Before the injection, the magnetic field and density fluctuations of all three modes grow and saturate due to the energy cascades from large to small spatial scales. After the

injection, the magnetic energy of Mode 1 decreases while that of Mode 2 increases, consistent with the PDI process. The density fluctuations of both Mode 1 and Mode 2 are very small. By using the dispersion relation analysis (e.g., Shi et al. 2017, Figure 8), we confirm that Mode 2 is an Alfvén wave because its frequency ($\omega = 0.088\Omega_i$) is close to $k_{\parallel}v_A = 0.091\Omega_i$ for $k_{\parallel} = 7k_0$. Despite fluctuation due to background turbulence, we fit the time series of wave power of fluctuating magnetic field or density to an exponential function $e^{\gamma t}$ to calculate growth rates. The growth rate of Mode 2 is estimated to be $\gamma/\Omega_i = 0.0022$ in the interval $600 < t\Omega_i < 1100$, smaller than the PDI growth rate in a quiescent plasma, which is $\gamma/\Omega_i = 0.0088$ (measured in Run 0, a simulation without background turbulence). The result confirms the reduction of PDI growth rate by turbulence found in previous MHD simulations (Shi et al. 2017). Since Mode 1 and 2 are Alfvén modes, their density fluctuation levels remain nearly unchanged. Meanwhile, δn of Mode 3 increases at a rate close to the growth rate of Mode 2 ($\gamma/\Omega_i = 0.0021$), but its magnetic field has no significant growth because of the characteristics of an ion acoustic mode. Dispersion relation analysis also confirms that Mode 3 has frequency $\omega = 0.035\Omega_i$, close to the ion acoustic frequency $k_{\parallel}c_s = 0.044\Omega_i$ for $k_{\parallel} = 17k_0$. For comparison, there is no growth of density or magnetic field fluctuation after $t\Omega_i = 500$ in Run 2 (no injection), as shown in Figures 3(c) and (d). After $t\Omega_i = 1200$, PDI saturates and the slow mode starts to decay at a rate $\gamma/\Omega_i = -0.0016$. This rate is about one-sixth of the Landau damping rate predicted by linear Vlasov theory (Gary 1993), which is $\gamma_L/\Omega_i = -0.01$ based on the plasma parameters at $t\Omega_i = 1200$. In a strongly turbulent environment, the assumptions of linear theory, including unperturbed charged particle orbits and uniform plasma distribution are no longer valid. In our simulation,

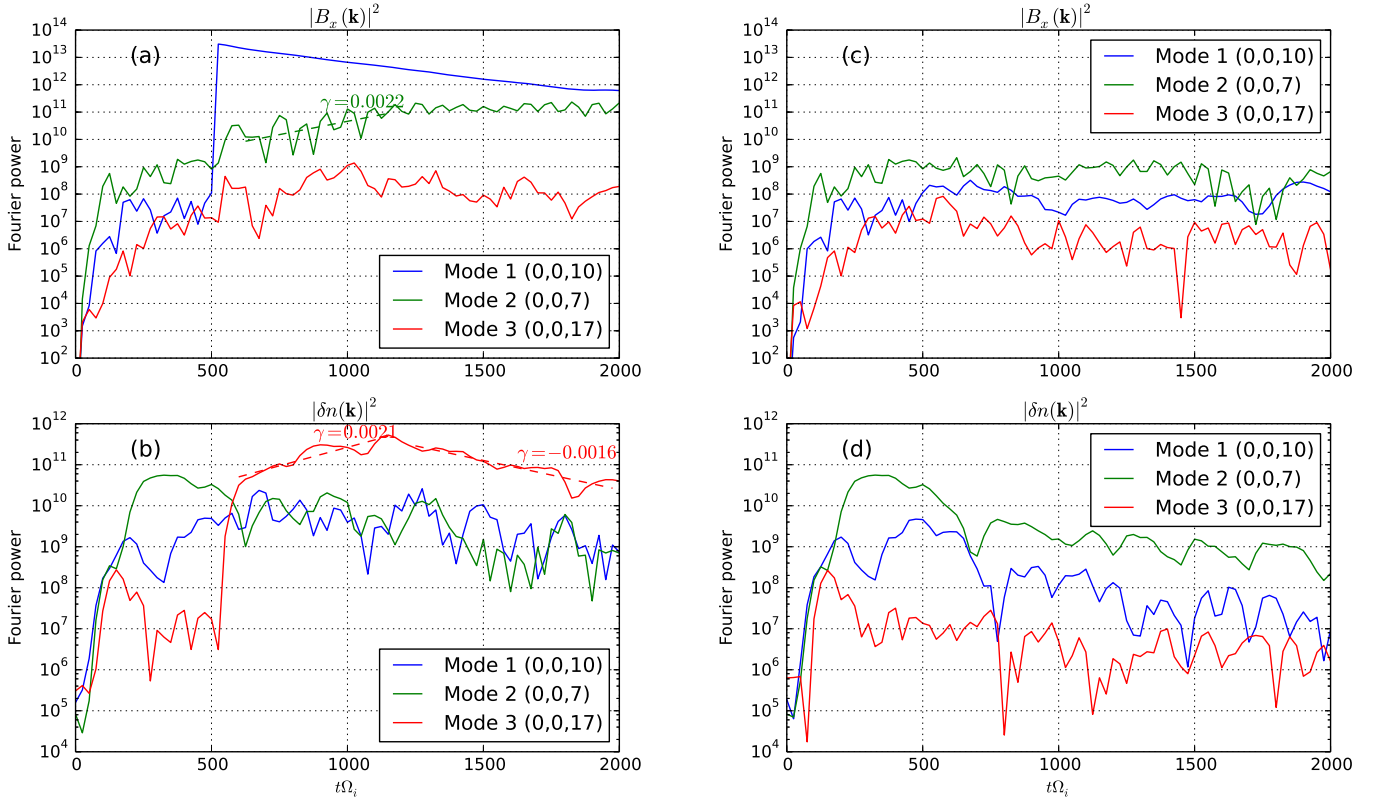


Figure 3. Time evolution of a wave power of (a) magnetic field B_x and (b) density δn in Run 1 for the three modes of interest $(k_x, k_y, k_z)/k_0 = (0, 0, 7); (0, 0, 10); (0, 0, 17)$. As a comparison, time evolution of wave power of B_x and δn in Run 2 (no injection) for the same three modes are shown in panels (c) and (d), respectively.

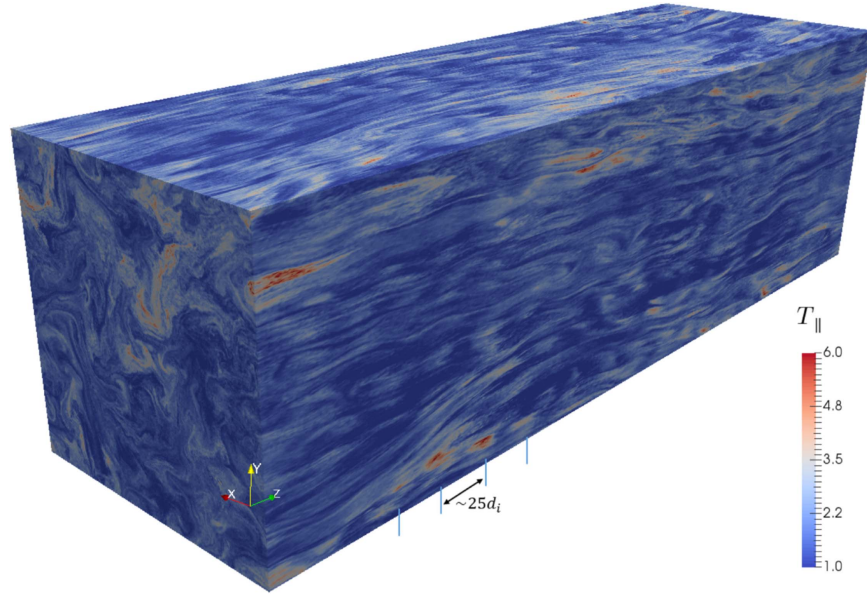


Figure 4. Surface contour plot of ion temperature $T_{\parallel}/T_{\parallel 0}$ at $t\Omega_i = 1000$ in Run 1. Localized ion heating leads to temperature enhancement structures whose parallel size is close to the wavelength of the slow mode predicted by the PDI theory.

strong density fluctuations shown in Figure 2(a) could be the main reason why the observed damping rate is much smaller than the theoretical prediction. Nevertheless, damping of the slow mode still leads to significant heating of ions in the parallel direction, which is also shown in Figure 2(a). Compared to Run 2, an additional 30% increase of ion temperature observed in Run 1 is due to the injection of the

Alfvén wave and subsequent damping of the slow mode. We obtain very similar results in simulations with 264 particles per cell (Run 3) and lower spatial resolution (Run 4), showing that the results are insensitive to numerical noise and resolution.

Figure 4 shows the surface contour of parallel ion temperature at $t\Omega_i = 1000$ in Run 1. Although the ion temperature distribution is also turbulent, temperature enhancement structures

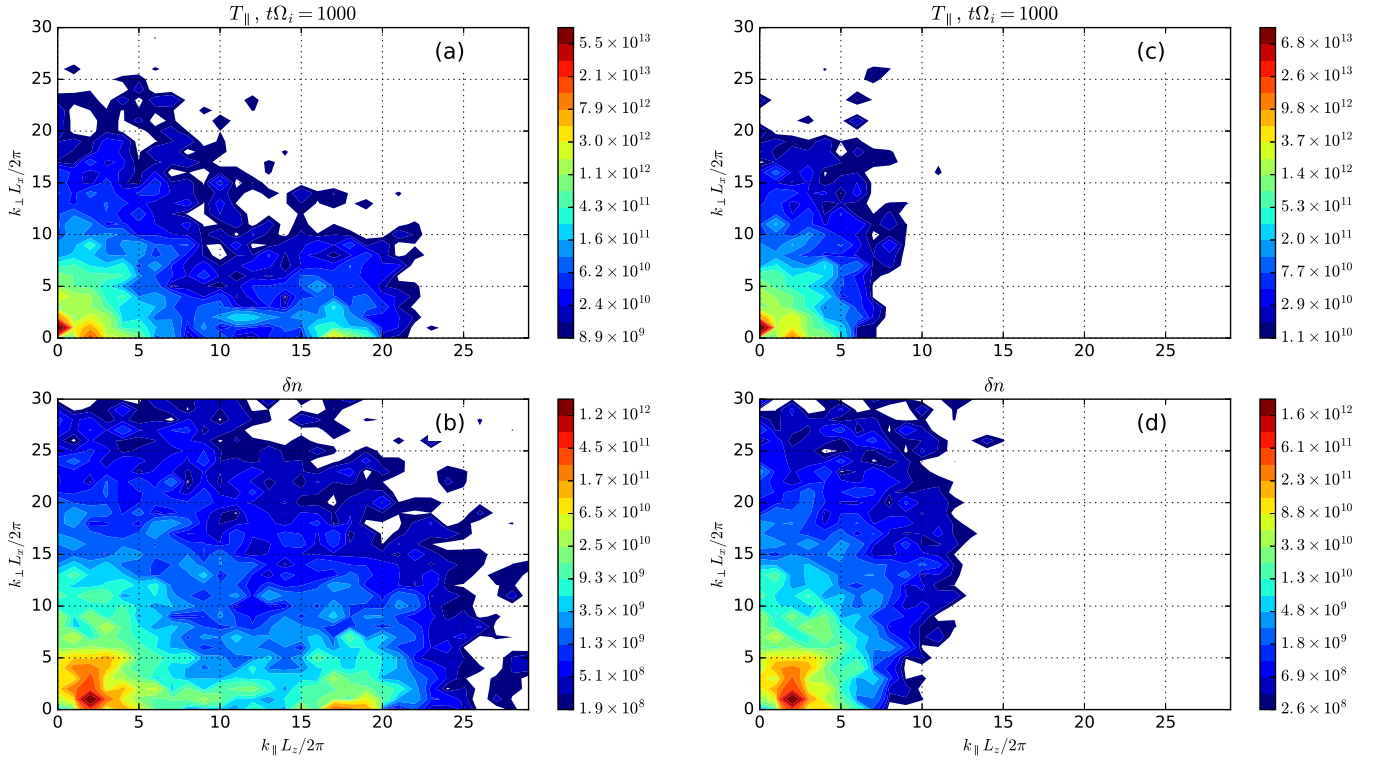


Figure 5. Power spectra of (a) parallel ion temperature T_{\parallel} and (b) density fluctuation δn as a function of k_{\parallel} and k_{\perp} at $t\Omega_i = 1000$ in Run 1. Localized structures in Figure 4 corresponding to wave number $k_{\parallel} L_z/2\pi = 17$, are associated with density fluctuation near mode $(0, 0, 17)$ produced by PDI. As a comparison, power spectra of T_{\parallel} and δn at $t\Omega_i = 1000$ in Run 2 (no injection) are shown in panel (c) and (d), respectively.

are observed in the simulation with local peaks $T_{\parallel}/T_{\parallel 0} \approx 10$ and parallel size ($\sim 25d_i$) close to the wavelength of the slow mode predicted by the PDI theory ($\sim 28d_i$). Fourier power spectra of the parallel ion temperature and density fluctuation at $t\Omega_i = 1000$ are shown in Figures 5(a) and (b), respectively. Clearly, the localized temperature enhancement structures in Figure 4 have a wave number $k_{\parallel} L_z/2\pi = 17$, and they are associated with density fluctuation near mode $(0, 0, 17)$ produced by PDI. Furthermore, there are strong oblique density fluctuations in long wavelength ($k_{\parallel} L_z/2\pi < 5$, $k_{\perp} L_x/2\pi < 5$ in Figures 5(a) and (b)) that are produced at the early stage of the simulation when turbulence is developing. They are also present in Run 2 (no injection), as shown in Figures 5(c) and (d). Their heating effect causes the surface contour of T_{\parallel} to appear localized in the perpendicular directions too. The structures are smoothed out later in the simulation, causing an overall heating of ions. Parallel velocity distributions ($v_{\parallel} \approx v_z$) of all ions in the simulation domain at different stages are shown in Figure 6. An initial Maxwellian velocity distribution has been significantly changed after the injection of wave and subsequent PDI through wave-particle interactions. Note that due to multiple Alfvén waves loaded initially, ion velocity distribution does not center at $v_z = 0$. Flattening of the distribution function occurs near $v_z/v_i \approx 1.0$ (where $v_i = v_A \sqrt{\beta_i}$ is the initial thermal speed of ions) around $t\Omega_i = 1000$ and near $v_z/v_i \approx 2.2$ around $t\Omega_i = 2000$. A noticeable amount of ions are accelerated to more than $2v_i$. Since the ion acoustic mode has a dispersion relation $\omega = k_{\parallel} \sqrt{(3T_i + T_e)/m_i} = 2k_{\parallel} v_i$, when $T_e = T_i$, the flattening of ion velocity distribution is consistent with ion Landau damping of the slow mode.

To study the possible excitation of PDI in low-beta solar wind plasmas near 1 au, we carry out further simulations with

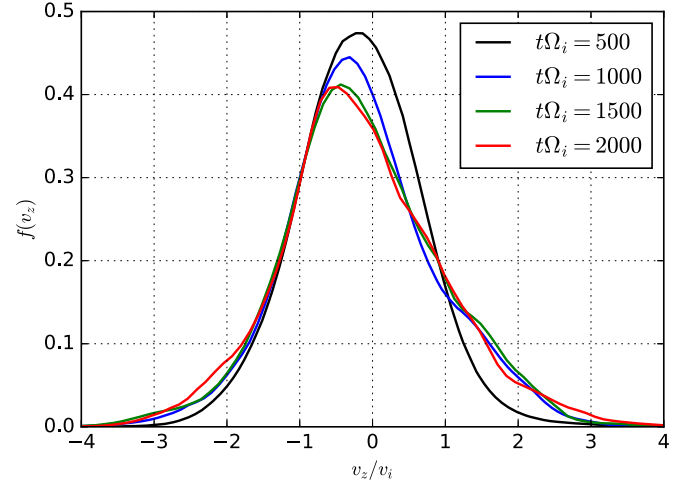


Figure 6. Ion velocity distribution $f(v_z)$ at various times in Run 1, where the velocity is normalized to the initial ion thermal velocity v_i and $v_z \approx v_{\parallel}$.

conditions motivated by observations (e.g., Shi et al. 2015; Li et al. 2016). Figure 2(b) shows results of Run 5 and 6, which initially have $\beta_i = 0.3$. When the background density perturbation drops to $\delta n/n \sim 0.1$ (note that δn^2 is multiplied by a factor of 2 in the figure), we inject an Alfvén wave with amplitude $\delta B/B_0 = 0.3$. Similar to Run 1 with $\beta_i = 0.01$, Run 5 shows features such as excitation of density fluctuations and parallel heating of ions after injection, consistent with PDI. Although in a plasma with higher beta, a higher amplitude Alfvén wave is needed to excite PDI (see Figure 1) and subsequent heating of ions is weaker, PDI is still shown to be effective with parameters relevant to the solar wind near 1 au. The presence of slow waves will also likely change the turbulent energy cascade in the parallel direction. All

of these effects suggest that turbulence and plasma heating in low-beta plasma deserve considerable additional efforts.

4. Discussion

In this paper, we use 3D hybrid simulations to study the PDI of a CPA wave in a turbulent low-beta plasma. It is shown that PDI is effective in such turbulence and the pump wave decays into another Alfvén wave and an ion acoustic wave, which is evident in the fluctuations of electromagnetic field and plasma density. The ion acoustic wave is subsequently damped through Landau resonance, causing significant heating of ions in the direction parallel to the background magnetic field. In low-beta plasmas, PDI provides an important channel for energy dissipation at a fluid scale, much larger than the ion kinetic scales in traditional turbulence models. It is often argued that parametric instabilities play a minor role in the development of turbulence in magnetized collisionless plasmas. For example, Howes (2015) argued that because of the anisotropic nature of plasma turbulence, i.e., turbulent fluctuations satisfy $k_{\parallel} \ll k_{\perp}$, the nonlinearity associated with Alfvén wave collisions (proportional to k_{\perp}) dominate over parametric instabilities, whose growth rates are proportional to k_{\parallel} . However, Equation (1) also shows that the growth rate of PDI correlates inversely with β . In low-beta plasmas, the growth of PDI can be faster than Alfvén wave collisions that are independent of β .





PDI may also play an important role in plasma heating inside interplanetary coronal mass ejections (Li et al. 2016), where plasma beta is observed to be on the order of 0.1 (Burlaga 1984). Near the transition region of the solar atmosphere, very low plasma beta (10^{-4} – 10^{-2} ; Gary 2001) makes PDI a potentially robust mechanism for solar corona heating (e.g., Pruneti & Velli 1997). We are expecting to see more direct evidence of PDI in the solar wind close to the Sun, which will be made available by the upcoming NASA Parker Solar Probe mission approaching as close as 8.5 solar radii from the Sun.

We have shown in a turbulent environment that PDI and Landau damping are still effective, although their growth or damping rates are reduced compared to the prediction of linear MHD theory or linear Vlasov theory in quiet plasmas. Turbulent fluctuations not only affect charged particle trajectories and background plasma density, invalidating the assumptions of linear theories, but also introduce effective collisions between charged particles in collisionless plasmas. Recently, Verscharen et al. (2017) analyzed in situ solar wind measurements and found that wave properties such as polarization of slow modes agree with MHD predictions better than the kinetic predictions, suggesting that the plasma behaves more like a fluid. This interesting behavior is worthy of further investigation using kinetic simulations, but it is beyond the scope of this paper.

The Los Alamos portion of this research was performed under the auspices of the U.S. Department of Energy. We are

grateful for support from the LANL/LDRD program and DOE/OFES. This research used resources provided by the Los Alamos National Laboratory Institutional Computing Program, which is supported by the U.S. Department of Energy National Nuclear Security Administration under Contract No. DE-AC52-06NA25396. Contributions from VR were supported by NASA grants NNX15AR16G and NNX14AI63G.

ORCID iDs

Xiangrong Fu  <https://orcid.org/0000-0002-4305-6624>
 Fan Guo  <https://orcid.org/0000-0003-4315-3755>
 Xiaocan Li  <https://orcid.org/0000-0001-5278-8029>
 Vadim Roytershteyn  <https://orcid.org/0000-0003-1745-7587>

References

- Burlaga, L. F. 1984, *SSRv*, **39**, 255
- Del Zanna, L., Matteini, L., Landi, S., Verdini, A., & Velli, M. 2015, *JPLPh*, **81**, 325810102
- Derby, N. F., Jr. 1978, *ApJ*, **224**, 1013
- Dorfman, S., & Carter, T. A. 2016, *PhRvL*, **116**, 195002
- Gao, X., Lu, Q., Li, X., Shan, L., & Wang, S. 2013a, *PhPI*, **20**, 072902
- Gao, X., Lu, Q., Tao, X., Hao, Y., & Wang, S. 2013b, *PhPI*, **20**, 092106
- Gary, G. A. 2001, *SoPh*, **203**, 71
- Gary, S. P. 1993, *Theory of Space Plasma Microinstabilities* (Cambridge: Cambridge Univ. Press)
- Goldreich, P., & Sridhar, S. 1995, *AJ*, **438**, 763
- Goldstein, M. L. 1978, *ApJ*, **219**, 700
- Howes, G. G. 2015, *RSPTA*, **373**, 20140145
- Howes, G. G., Bale, S. D., Klein, K. G., et al. 2012, *ApJL*, **753**, L19
- Karimabadi, H., Vu, H. X., Krauss-Varban, D., & Omelchenko, Y. 2006, in *ASP Conf. Ser. 359, Numerical Modeling of Space Plasma Flows*, ed. N. V. Pogorelov & G. P. Zank (San Francisco, CA: ASP), 257
- Kellogg, P. J., & Horbury, T. S. 2005, *AnGeo*, **23**, 3765
- Li, H., Wang, C., Belcher, J. W., He, J., & Richardson, J. D. 2016, *ApJL*, **824**, L2
- Makwana, K., Li, H., Guo, F., & Li, X. 2016, 1 arXiv:1608.07829
- Makwana, K. D., Zhdankin, V., Li, H., Daughton, W., & Cattaneo, F. 2015, *PhPI*, **22**, 042902
- Malara, F., Primavera, L., & Veltri, P. 2000, *PhPI*, **7**, 2866
- Matteini, L., Landi, S., Del Zanna, L., Velli, M., & Hellinger, P. 2010, *GeoRL*, **37**, 2
- Narita, Y., & Glassmeier, K. 2007, *NPGeo*, **14**, 361
- Oughton, S., Matthaeus, W. H., Wan, M., & Osman, K. T. 2015, *RSPTA*, **373**, 20140152
- Podesta, J. J., & Roytershteyn, V. 2017, *JGRA*, **122**, 6991
- Pruneti, F., & Velli, M. 1997, in *Fifth SOHO Workshop: The Corona and Solar Wind Near Minimum Activity*, ed. A. Wilson (Noordwijk: ESA), 623
- Sagdeev, R. Z., & Galeev, A. A. 1969, *Nonlinear Plasma Theory* (New York: Benjamin)
- Shi, M., Li, H., Xiao, C., & Wang, X. 2017, *ApJ*, **842**, 63
- Shi, M. J., Xiao, C. J., Li, Q. S., et al. 2015, *ApJ*, **815**, 122
- Spangler, S. R., Leckband, J. A., & Cairns, I. H. 1997, *PhPI*, **4**, 846
- Tenerani, A., & Velli, M. 2013, *JGRA*, **118**, 7507
- Tu, C. Y., & Marsch, E. 1995, *SSRv*, **73**, 1
- Verscharen, D., Chen, C. H. K., & Wicks, R. T. 2017, *ApJ*, **840**, 106
- Yao, S., He, J.-S., Tu, C.-Y., Wang, L.-H., & Marsch, E. 2013, *ApJ*, **774**, 59
- Zanna, L. D. 2001, *GeoRL*, **28**, 2585
- Zhdankin, V., Werner, G. R., Uzdensky, D. A., & Begelman, M. C. 2017, *PhRvL*, **118**, 055103